Progress In Electromagnetics Research C, Vol. 8, 161–177, 2009

FULL-WAVE INVESTIGATIONS OF A PROBE-EXCITED RECTANGULAR RING ANTENNA BY METHOD OF MOMENTS WITH RWG BASIS FUNCTIONS

S. Lamultree

Faculty of Engineering and Technology
Asian University
Chon Buri 20250, Thailand

C. Phongcharoenpanich

Faculty of Engineering
King Mongkut's Institute of Technology Ladkrabang
Bangkok 10520, Thailand

Abstract—Radiation pattern, impedance characteristics, and gain of a probe-excited rectangular ring antenna are investigated by the Method of Moments with the Rao-Wilton-Glisson (RWG-MoM) basis functions. The analysis is carried out for different lengths and positions of the probe as well as various lengths, widths and heights of the ring. In addition, the distribution of the surface current is also illustrated. Consequently, the suitable parameters are determined. It is obvious that the proposed antenna offers a bidirectional pattern with the impedance bandwith ($|S_{11}| < -10\,\text{dB}$) of 17%. Along the direction of the ring aperture, the gain is 5.28 dBi. Furthermore, the prototype antenna was fabricated and measured to verify the validity of the numerical calculation. It is found that the numerical and measured results are reasonably in good agreement.

1. INTRODUCTION

Recently, the wireless communications become essential in human activity. Therefore, the demand for using a mobile telephone is increased everywhere. Generally, the base station antennas in microcellular system for the urban areas are located lower than the surrounded buildings along the streets, and sometimes they are located

Corresponding author: S. Lamultree (suthasineel@asianust.ac.th).

in the underground areas. Many base stations are placed indoors such as in the building, underground shopping areas and subway station. In these circumstances, the communicable cell is formed along the street. For these environments, a bidirectional antenna is more suitable to apply serving these demands. In addition, bidirectional antennas can be enlarged the cell size along the street in microcell environment [1, 2]. Therefore, many researches and developments on bidirectional antennas have been extensively conducted [3–10]. Nevertheless, the low cost must be considered since the number of cell is very large. Hence, the probe-excited different ring shapes, such as rectangular, circular, elliptical rings, are introduced [6–10]. The omnidirectional pattern of linear probe is forced by the surrounded rings to provide the bidirectional pattern. Because of the simple structure, the bidirectional rectangular ring was presented in [6, 8, 9] to be used as a base station antenna at the narrow and long path serviced areas. It is also possible to adjust the beamwidth of the antenna corresponding to the applications by changing the ring width and ring height. Furthermore, the desired directivity is easily obtained by varying the ring length.

Theoretically, there are many techniques to analyze the radiation from the aperture fed by probe in open literatures [11–17]. The dyadic Green's function approach [16–21] is used to analyze the radiation characteristics of the probe-excited rectangular ring antenna [9] because it is straightforward; in addition that the closed form solutions are obtained. The fields inside the rectangular ring, equivalent electric and magnetic current densities on the aperture, and far field radiations were expressed. Nevertheless, the analysis is performed under the assumption that the current is assumed to be sinusoidal distribution, the mutual coupling between the two apertures and the diffraction at the edge of the ring are neglected. The input impedance that is very sensitive to the actual current is not accurately achieved under those assumptions. Therefore, the full-wave analysis is necessary. The Method of Moments with the Rao-Wilton-Glisson (RWG-MoM) basis functions [22–25] is the suitable choice to solve the surface integral equations for arbitrarily shaped objects. Its basis functions include not only for each member of patch which contains an edge lying on the boundary of the unit cell, but also the adjacent face-pairs of the triangulated surface. The accurate solutions of the impedance characteristics including radiation pattern and gain are accomplished. In this paper, the RWG-MoM is applied to investigate the characteristics of the proposed antenna. Using this approach, the antenna surface is divided into a number of triangular patches. Hence, the criterion of convergence should be carefully considered before

computing. Subsequently, the influences of the antenna parameters are investigated to obtain the suitable ones.

This paper is organized as follows. The electrical field formulations are expressed in Section 2. In Section 3, antenna structure and numerical results are shown. Then, the antenna design and experimental results are presented in Section 4. Finally, conclusions are provided in Section 5.

2. ELECTRIC FIELD FORMULATIONS

In terms of RWG basis function $\bar{f}_n$ [24], the surface electric current density $\bar{J}$ on the metal surface divided into triangular patches is given as

$$\bar{J} \cong \sum_{n=1}^{N} I_n \bar{f}_n(\bar{r}) \tag{1}$$

where N is the number of interior (non-boundary) edges. Since a basis function is associated with each non-boundary edge of the triangulated structure, up to three basis functions may have nonzero values within each triangular face. For a given edge, only the basis function associated with that edge has a current component normal to the edge; all other basis currents in adjacent faces are parallel to the edge. Furthermore, since the normal component of $\bar{f}_n$ at the nth edge is unity, each expansion coefficient I_n may be interpreted as the normal component of current density flowing pass the nth edge. Also, the basis functions in each triangle are independent, because the current normal to the nth edge that is an independent quantity. Due to the current continuity, the summation of normal components of currents on opposite sides of the surface boundary edges is cancelled. Therefore, it is neither defined nor included in (1) contributions from basis function associated with such edges.

Once the surface currents are known, the electric and magnetic fields in everywhere of the space can be found using either surface integrals or elegant dipole model. Assuming that every RWG edge element behaves like a dipole of constant current located between the centroids of the triangle adjacent to each edge. To find the equivalent moment, considering a RWG element m with two inner triangle edges of $T_m^{\pm}$ adjacent to the edge of length l_m, the dipole moment $\bar{m}$ producing from the products of an effective dipole current is obtained by integration of the surface current as

$$\bar{m} = \int\limits_{T_m^+ + T_m^-} I_m \bar{f}_m(\bar{r}) dS = l_m I_m (\bar{r}_m^{c_0-} - \bar{r}_m^{c_0+}) \tag{2}$$

where c_0 denotes the triangular midpoint. $\bar{f}_m(r)$ is the RWG basis function corresponding to the element m. An effective length of dipole l is given by $[\bar{r}_m^{c_0-} - \bar{r}_m^{c_0+}]$. Consequently, the coefficient of surface current I_m is determined from the moment equations as

$$[Z_{mn}]\left[\bar{I}_n\right] = \left[\bar{V}_m\right] \tag{3}$$

where $[Z_{mn}]$ is an impedance matrix $N \times N$. $\bar{I}_n$ and $\bar{V}_m$ are the vector of expansion coefficients and the applied voltage vector, respectively. It is note that the feeding voltage of 1 V is assumed.

The radiation electric and magnetic fields of an infinitesimal dipole at the point $\bar{r}$ are

$$\bar{E}(\bar{r}) = \frac{j\eta}{4\pi}\left(\left(\bar{M} - \bar{m}\right)\left[\frac{jk}{r} + C\right] + 2\bar{M}C\right)e^{-jkr} \tag{4}$$

$$\bar{H}(\bar{r}) = \frac{jk}{4\pi}(\bar{m} \times \bar{r})Ce^{-jkr} \tag{5}$$

where $\bar{M} = \frac{(\bar{r}\cdot\bar{m})\bar{r}}{r^2}$ and $C = \frac{1}{r^2}\left[1 + \frac{1}{jkr}\right]$.

3. ANTENNA DESIGN

The antenna structure and the parametric study are shown in this section. The parameters that affect the radiation pattern, impedance characteristic and gain are investigated.

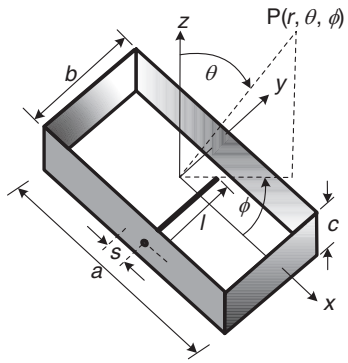

Figure 1. A probe-excited rectangular ring antenna.

3.1. Antenna Structure

Figure 1 shows the structure of the probe-excited rectangular ring antenna. It consists of the ring width a, ring height b and ring length c that surrounds a linear probe of the length l. Considered that the probe aligns along y direction at the position of ($x = s$, $y = -b/2$, $z = 0$), where s is the distance of probe offset from the centre ($x = 0$, $y = -b/2$, $z = 0$).

3.2. Parametric Study

The characteristics of the antenna depend on the following parameters, i.e., the ring width (a), the ring height (b), the ring length (c), the probe length (l) and the probe position (s). Since the cross-section of the antenna is the same as a rectangular waveguide, in this circumstance the ring width and ring height are chosen to be the dimension of a standard waveguide operating at the dominant mode (TE_{10}). Therefore, the ring width of a, and ring height of b are initially selected as $a = 0.70\lambda$ and $b = 0.35\lambda$. Accordingly, the antenna characteristics depend on the ring length, probe length and probe position. In the preliminary study, the initial probe length of 0.25λ is selected for the reason of impedance matching (the suitable length is determined later). To study the effect of each parameter, the RWG-MoM is used. Applying this method, the antenna structure in Figure 1 is modeled from a number of triangular patches as shown in Figure 2(a) feeding with a thin strip instead of a cylindrical one to avoid the separate algorithms of wire and patch models as shown in Figure 2(b). Note that, in general, a thin strip width of excited probe should be 4 times of the radius of the equivalent cylindrical structure [24]. The material of the antenna is made by copper with conductivity of 5.8×10^7 S/m.

Before starting to calculate, it is worthwhile to consider the number of triangular segments that uses to model the antenna by using the criterion of convergence that the deviation of input impedance of the antenna is less than 0.1% as shown in Figure 3. It is found that when the number of triangle is increased, the less deviation is achieved. In this paper, the number of triangular segments of 1,894 RWG basis functions is used.

Figure 4 shows the radiation patterns of the probe-excited rectangular ring antenna for various ring lengths (c). It is found that a bidirectional pattern can be produced due to the confinement of linear probe by rectangular ring. In addition, the separation between the two apertures or the ring length has been strongly influenced to the radiation pattern. In the yz-plane, the beamwidth is widened

and then split when the ring length is increased. After that, the bidirectional pattern with the existed side lobes is achieved again at $c = 1.25\lambda$. By varying the ring lengths, it is found that the shorter ring length provides the wide beamwidth in the xz-plane because the aperture separation affects the radiation patterns. In addition,the radiation pattern has null at $\theta = 90°$ in the yz- and xz-planes due to the ring edge effecting. It is observed that the dyadic Green's function approach [9] and the RWG-MoM provide the same trend of radiation pattern. However, using the RWG-MoM, the beamwidths of the antenna are narrower and its null is deeper than that using the

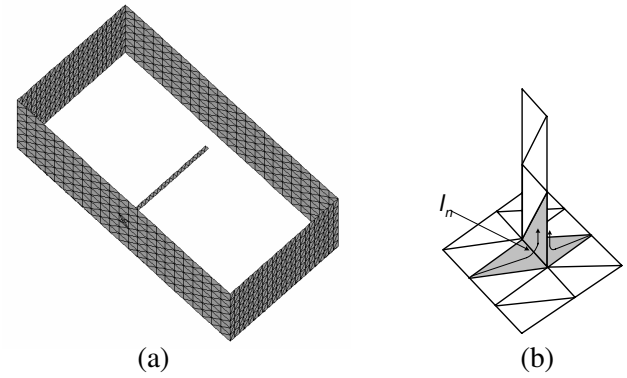

Figure 2. Antenna model: (a) A probe-excited rectangular ring antenna, and (b) probe-excitation.

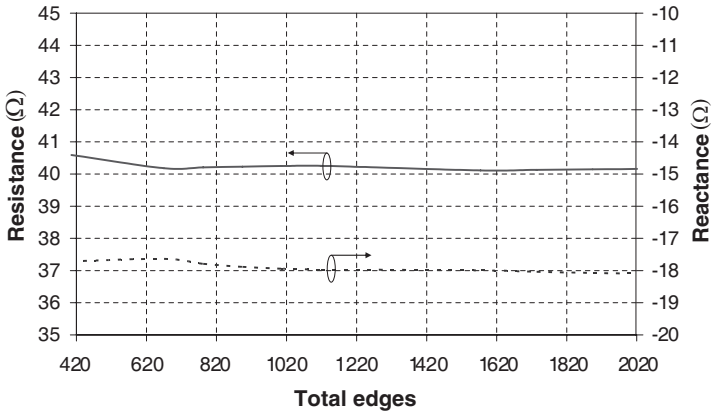

Figure 3. Convergence criteria.

dyadic Green's function approach. The reason is due to the mutual effect between the two apertures and the diffraction from the edges are not taken into account.

To consider the impedance matching between the antenna and coaxial transmission line (with characteristic impedance of $50\,\Omega$), the impedance characteristic is shown in terms of $|S_{11}|$ versus the probe length (l) for different ring lengths c of 0.15λ, 0.20λ, 0.25λ, 0.30λ and 0.40λ respectively, as plotted in Figure 5(a). It is found that almost all cases provide good matching condition at probe length of 0.27λ with $|S_{11}|$ of $-21.62\,\text{dB}$, $-27.29\,\text{dB}$, $-30.46\,\text{dB}$, $-27.25\,\text{dB}$ and $-20.38\,\text{dB}$ for c of 0.15λ, 0.20λ, 0.25λ, 0.30λ and 0.40λ, respectively ($c = 0.15\lambda$ and $c = 0.40\lambda$ provide the lowest $|S_{11}|$ at $-21.96\,\text{dB}$ and $-22.00\,\text{dB}$ corresponding to $l = 0.26\lambda$). Therefore, the probe length of 0.27λ is chosen and fixed hereafter. In addition, Figure 5(b) shows the gain for various ring lengths versus probe length. Obvious that the increasing gains are provided as the longer probe length. The gains are maximum at $l = 0.27\lambda$ for c of 0.15λ, 0.20λ, 0.25λ and 0.30λ, and $l = 0.26\lambda$ for the c of 0.40λ. For the longer probe length, the gains are decreased. For $l < 0.19\lambda$, the gains are relatively low due to the strong reflection between the antenna and the transmission line because the input impedance is remarkably deviated from $50\,\Omega$. Furthermore, the maximum gains at $l = 0.27\lambda$ of 4.92 dBi, 5.22 dBi, 5.28 dBi and 5.20 dBi are obtained for c of 0.15λ, 0.20λ, 0.25λ and 0.30λ, respectively, and at $l = 0.26\lambda$ the gain of 4.70 dBi is obtained for c of 0.40λ. Comparing the

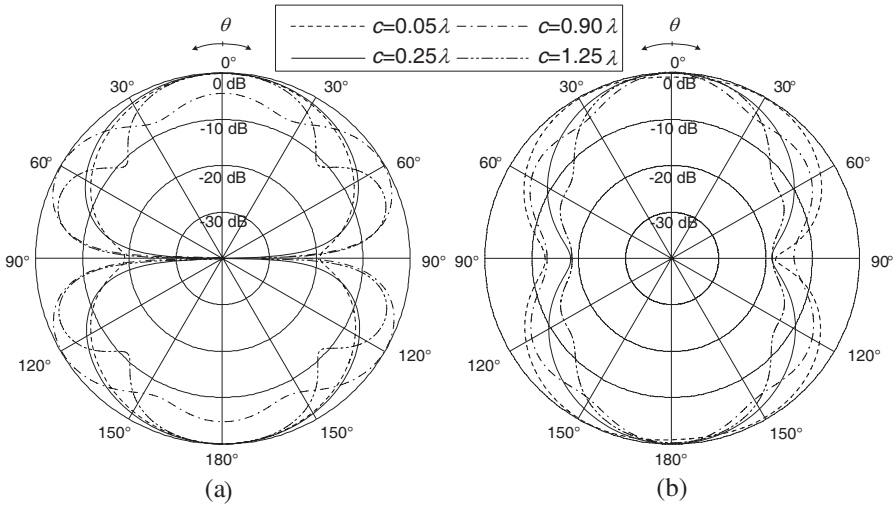

Figure 4. Radiation pattern: (a) yz-plane and (b) xz-plane.

gain for different c, it is found that the ring length of 0.25λ provides the maximum gain and the optimum matching condition.

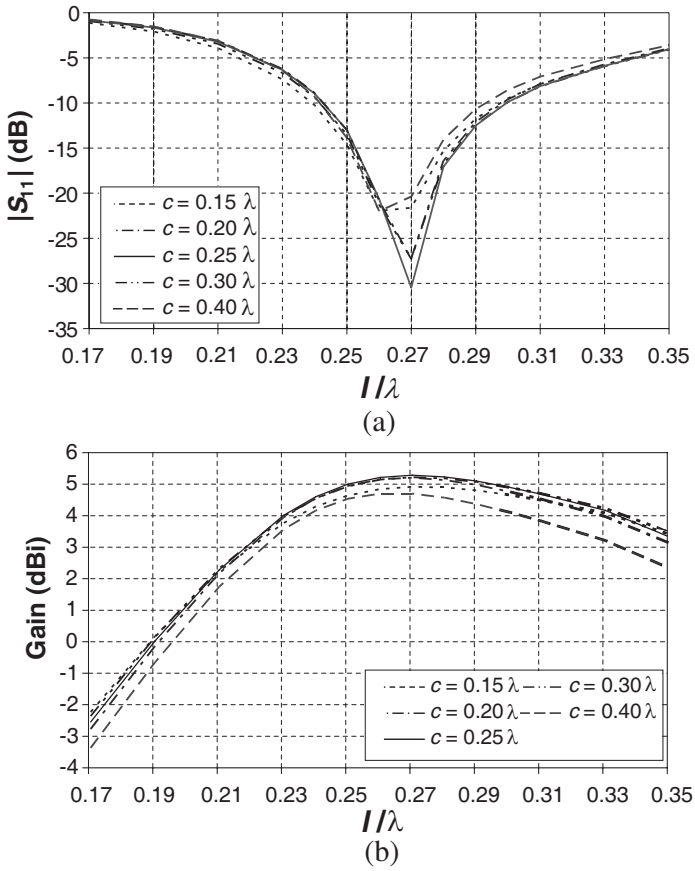

Figure 5. $|S_{11}|$ and gains versus probe length: (a) $|S_{11}|$, and (b) gains.

Furthermore, the frequency response of $|S_{11}|$ and gain are plotted as shown in Figure 6. It is found that the impedance bandwidth covers 17% ($|S_{11}| < -10\,\text{dB}$) with the resonant frequency slightly shifted from the operating frequency for mostly ring lengths as shown in Figure 6(a) except for the case that $c = 0.4\lambda$, it is resonated at $0.98f_0$ with the impedance bandwidth of 15%. This is due to the resonant frequency of the antenna is affected by both the probe excitation and the rectangular ring. Furthermore, along the direction of the ring aperture ($\theta = 0°$, $\phi = 90°$), the gain of different ring lengths are plotted

versus frequency as shown in Figure 6(b). Apparently, the increasing gains are obtained for the increasing frequency. The maximum is achieved at the operating frequency f_0 for c of 0.20λ, 0.25λ and 0.30λ, and the frequency of $0.98f_0$ for c of 0.15λ and 0.40λ, respectively. Moreover, the ring length c of 0.25λ provides the maximum gain of 4.50–5.28 dBi along the frequency band of $0.90f_0$–$1.10f_0$ (the difference between the maximum and minimum gain is less than 3 dB). It is apparent that the ring lengths of 0.40λ yields the minimum gain of 3.41–4.76 dBi. At the operating frequency, the ring lengths of 0.15λ, 0.20λ, 0.25λ, 0.30λ and 0.40λ provide the gains of 4.92 dBi, 5.22 dBi, 5.28 dBi, 5.20 dBi and 4.76 dBi, respectively. As the results, the ring length of 0.25λ is selected because the gain is maximum.

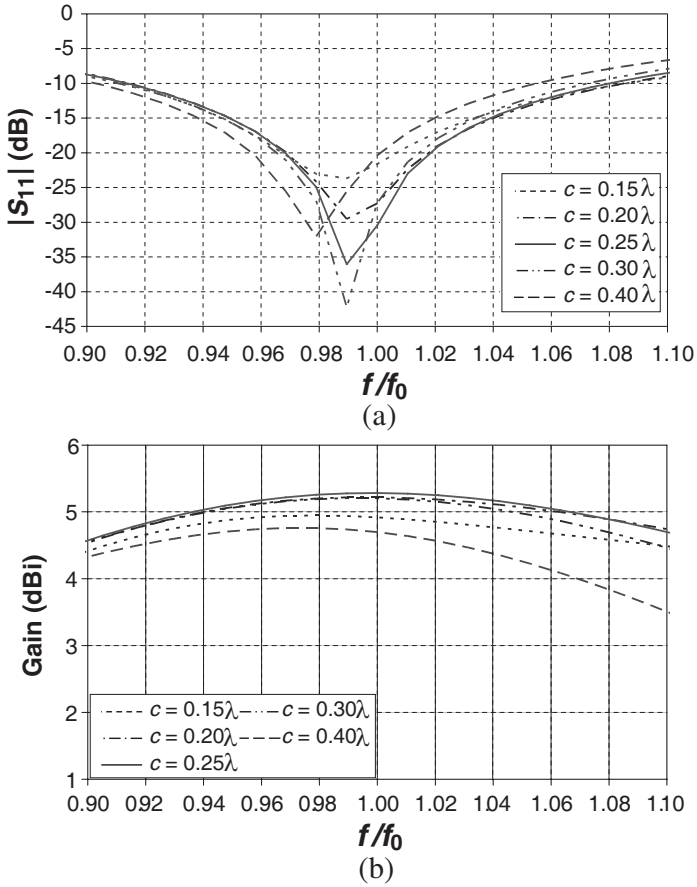

Figure 6. Frequency response of: (a) $|S_{11}|$ and (b) gains.

In addition to the probe length, the effect of probe position (s) to $|S_{11}|$ and gain is also considered and plotted as shown in Figure 7. It is found that $|S_{11}|$ and gain have the opposite curve; i.e., $|S_{11}|$ is increased as further distance of s from the center ($x = 0$, $y = -b/2$, $z = 0$) where the trend of gain is decreased. The matched condition is obtained when $s < 0.11\lambda$. At the center ($s = 0$, $y = -b/2$, $z = 0$), the optimum matched impedance with $|S_{11}|$ of -30.46 dB is observed. From Figure 7, the gain is further decreased for $s > 0.11\lambda$ due to the mismatched impedance. However, the gain is slightly decreased when $s < 0.11\lambda$ with the matched impedance ($|S_{11}| < -10$ dB). It should be pointed that the probe position has strong effect to impedance characteristic and gain.

Figure 8 shows the influence of b/a to the input impedance and $|S_{11}|$ when l is fixed at 0.27λ. Apparently, the increasing $|S_{11}|$ is seen for the higher ratio of b/a. However, The level of $|S_{11}|$ is lower than -10 dB for b/a of 0.4–1.0. The lowest $|S_{11}|$ of -41.23 dB is obtained at $b/a = 0.45$ with the corresponding impedance of $50.17–j0.85\,\Omega$. From Figure 8, it is shown that the impedance characteristics have been strong affected from the probe-excitation rather than the ring dimension. The variation of b/a (with the fixed probe length) have weak effect to the impedance characteristics.

Furthermore, surface current distributions of the antenna are illustrated as shown in Figure 9. Obviously, the maximum current occurs at the feed point, and it is dense along a linear probe. Accordingly, the radiation fields are mainly produced from the linear probe, and then its radiation pattern is confined by rectangular ring

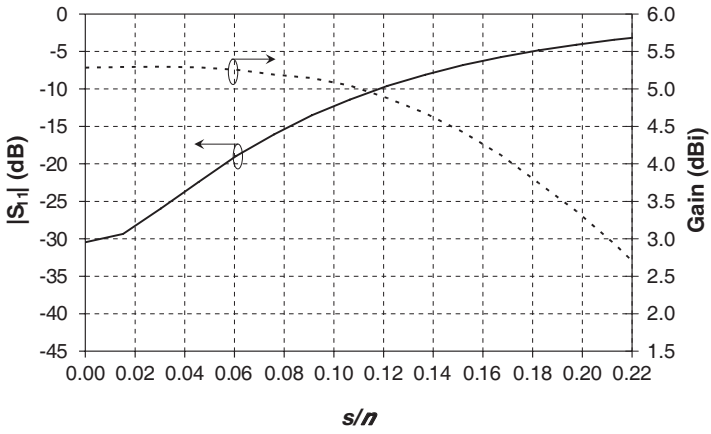

Figure 7. $|S_{11}|$ and gain for various s.

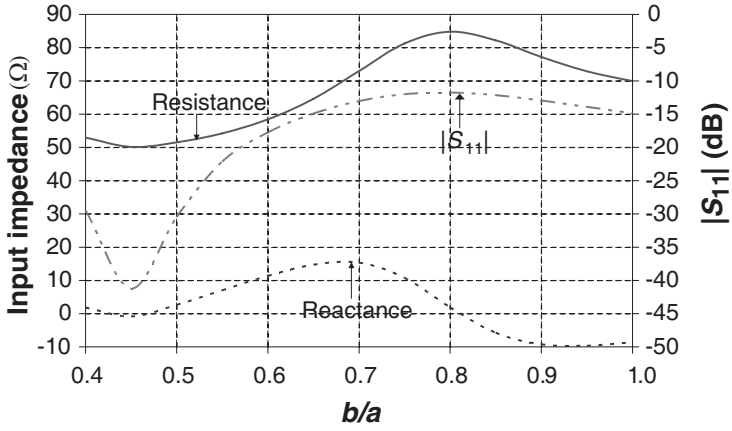

Figure 8. Input impedance and $|S_{11}|$ for various b/a when $l = 0.27\lambda$.

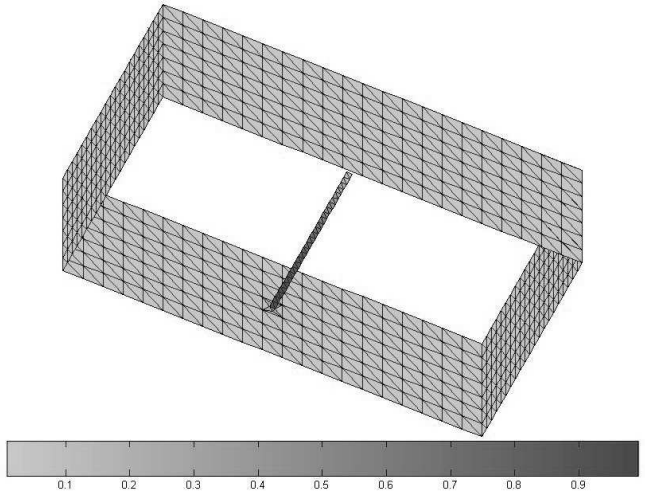

Figure 9. Current distributions.

providing bidirectional beam in the forward and backward directions along the ring aperture. In addition, it should be pointed that a linear probe has strong effect to the impedance of the antenna.

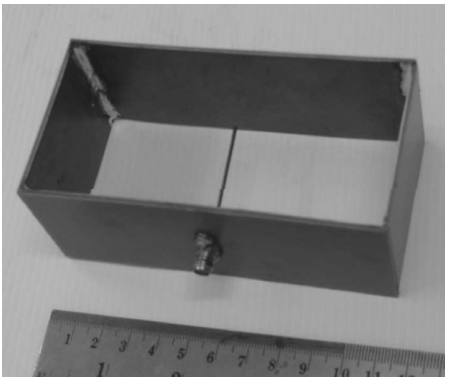

Figure 10. Photograph of the prototype antenna.

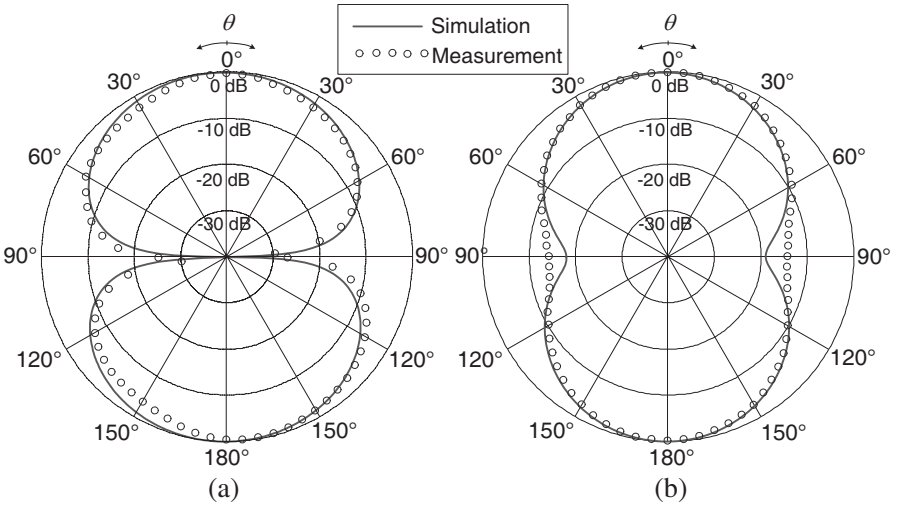

Figure 11. Calculated and measured radiation patterns: (a) yz-plane and (b) xz-plane.

4. MEASUREMENTS

To confirm the numerical calculation, the prototype antenna was fabricated with the designed parameters from the preceding section at the operating frequency of 1.9 GHz. The ring was made of copper with 1 mm thickness. The ring height, ring width and ring length are 55 mm, 110 mm and 39 mm, respectively. The antenna was fed by the linear probe that was made from the copper rod of the diameter

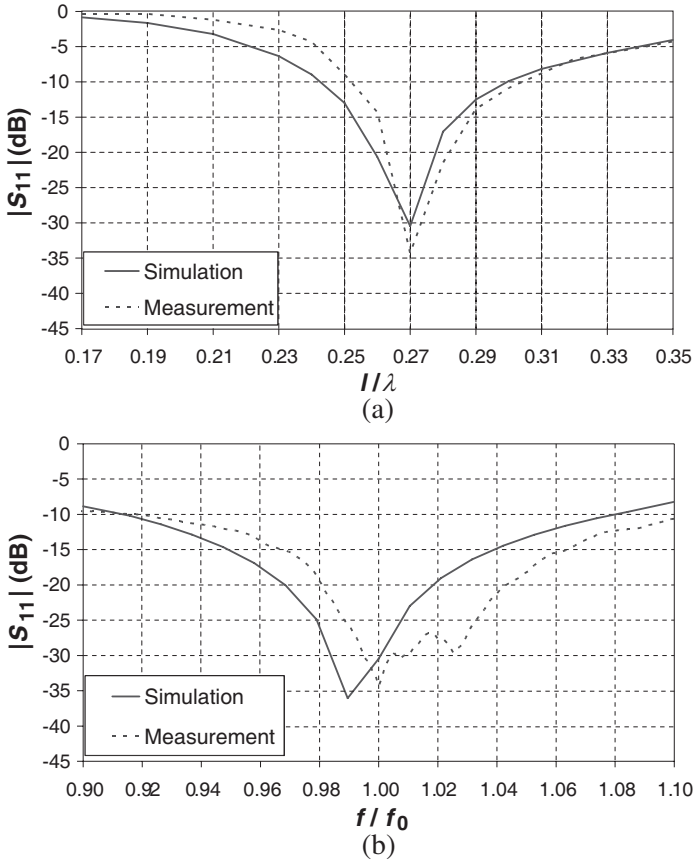

Figure 12. Comparison the calculated and measured $|S_{11}|$: (a) Versus probe length (b) versus frequency.

0.65 mm. The probe length is 43 mm. This probe was connected to the transmission line via the SMA connector. The photograph of the fabricated antenna is depicted in Figure 10.

Using an HP8720C Network Analyzer, the radiation pattern, the impedance characteristic in terms of $|S_{11}|$, and the gain were measured. The calculated and measured radiation patterns in yz-plane and xz-plane are shown in Figure 11(a) and Figure 11(b), respectively. Obviously, the maximum radiated field directs along the ring aperture in $+z$ and $-z$ directions. In addition, the radiation pattern in yz-plane tilts from z axis because the linear probe is located at the bottom of the ring making unsymmetrical structure along yz-plane. The beam peak in yz-plane of the theory and measurement directs at 3 and 0 degrees

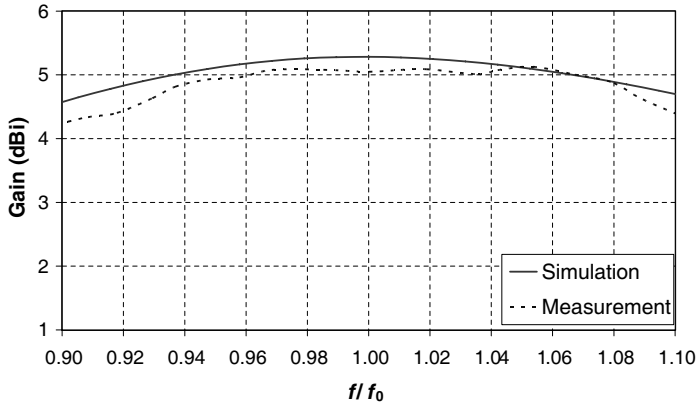

Figure 13. The calculated and measured gains.

with the calculated and measured half-power beamwidths of 88 and 95 degrees, respectively. For the symmetrical structure along xz-plane, the radiation pattern is symmetry in this plane. In xz-plane, the beam peaks of both theory and measurement direct at 0 degree with the calculated and measured half-power beamwidths of 66 and 74 degrees, respectively. The theory and measurement are in good agreement.

In addition, the matching impedances between coaxial transmission line (with the characteristic impedance of 50 Ω) and the antenna are plotted in terms of $|S_{11}|$ as shown in Figure 12. Apparently, the theory and measurement provide the lowest $|S_{11}|$ at $l = 0.27\lambda$ with $|S_{11}|$ of -30.46 dB and -34.32 dB, respectively, as shown in Figure 12(a). Moreover, in Figure 12(b), the calculated and measured impedance bandwidths of 17% and 18% for the $|S_{11}| < -10$ dB are obtained, respectively. It is found that the resonant frequencies are yielded at $0.99f_0$ and f_0 for the theory and measurement, respectively. When comparing between the theory and measurement, they are in good agreement.

The gain of the antenna was also measured and plotted compared with the theory as shown in Figure 13. It is found that the calculated and measured gains at the direction of $\theta = 0^\circ$ and $\phi = 90^\circ$ along the frequency ranging from $0.90f_0$ to $1.10f_0$ are 4.50–5.28 dBi and 4.19–5.13 dBi, respectively. The minimum and maximum gains from the theory are obtained at the $0.90f_0$ and f_0 with gains of 4.58 dBi and 5.28 dBi, respectively, whereas the minimum and maximum gains from the measurement are yielded at the $0.90f_0$ and $1.05f_0$ with gains of 4.25 dBi and 5.13 dBi, respectively. At the operating frequency, the gains of 5.28 dBi and 5.05 dBi are obtained from the theory and

measurement, respectively. Obviously the theory and measurement possess the acceptable agreement.

5. CONCLUSION

This paper presents the full-wave investigation of a probe-excited rectangular ring antenna by using the RWG-MoM. This technique is suitable for modeling the metallic surface problem. Using RWG-MoM, the antenna is modeled by dividing the antenna surfaces into a number of triangular patches of 1,896 segments associated with the deviation of input impedance of the antenna is less than 0.1%. Then, the radiation pattern, the impedance characteristic in terms of $|S_{11}|$ and gain are investigated for various length and position of probe with different ring length. Along the direction of ring aperture, it is found that the ring length of 0.25λ with the probe length of 0.27λ located at the center ($x = s = 0$, $y = -b/2$, $z = 0$) provides the maximum calculated and measured gains of 5.28 dBi and 5.05 dBi, respectively. The achieved optimum impedance matching from calculation and measurement in terms of $|S_{11}|$ are -30.46 dB and -34.32 dB, respectively. Moreover, the calculated and measured impedance bandwidths of 17% and 18% for the $|S_{11}| < -10$ dB are obtained. By using delta gap voltage excitation, it is found that the current distributes along the probe excitation. The radiation from the probe is confined by the rectangular ring to provide the bidirectional pattern. In addition, the impedance characteristic and gain have been stronger affected from the probe excitation than the rectangular ring. To verify the theoretical results, the prototype antenna was fabricated and measured. It is found that the calculation and measurement are reasonably in good agreement.

ACKNOWLEDGMENT

This work was supported by the Thailand Research Fund (TRF) under the grant number RSA5080009.

REFERENCES

1. Arai, H., "Base station antennas inside tunnels and subway stations, and outdoor compact base station antennas for PDC system in Japan," *The Proceedings of IEEE Antennas and Propagation Society International Symposium*, Vol. 1, 568–571, 1999.

2. Arai, H. and K. Cho, "Cellular and PHS base station antenna systems," *IEICE Transactions on Communications*, No. 9, 980–992, 2003.
3. Cho, K., T. Hori, H. Tozawa, and S. Kiya, "Bidirectional rod antennas comprising collinear antenna and parasitic elements," *IEICE Transactions on Communications*, No. 6, 1255–1260, 1998.
4. Cho, K., T. Hori, and K. Kagoshima, "Bidirectional rod antennas comprising a narrow patch and parasitic elements," *IEICE Transactions on Communications*, No. 9, 2482–2489, 2001.
5. Liu, H., B.-Z. Wang, and W. Shao, "Dual-band bi-directional pattern reconfigurable fractal patch antenna for millimeter wave application," *International Journal of Infrared and Millimeter Waves*, Vol. 28, No. 1, 25–31, 2007.
6. Kosulvit, S., C. Phongcharoenpanich, M. Krairiksh, and T. Wakabayashi, "Radiation characteristics of a bidirectional antenna using a linear probe in a rectangular ring," *The Proceedings of International Conference on Microwave and Millimeter Wave Technology*, 337–340, 1998.
7. Kosulvit, S., M. Krairiksh, C. Phongcharoenpanich, and T. Wakabayashi, "A simple and cost-effective bidirectional antenna using a probe excited circular ring," *IEICE Transactions on Electronics*, Vol. E84-C, No. 4, 443–450, 2001.
8. Lamultree, S., C. Phongcharoenpanich, S. Kosulvit, and M. Krairiksh, "Investigations of a bidirectional antenna using a probe excited rectangular ring," *The Proceedings of Asia-Pacific Microwave Conference 2005*, Vol. 5, 2943–2946, 2005.
9. Lamultree, S., C. Phongcharoenpanich, S. Kosulvit, and M. Krairiksh, "Analysis of radiation characteristics of a probe-excited rectangular ring antenna by the dyadic Green's function approach," *Progress In Electromagnetics Research B*, Vol. 11, 79–101, 2009.
10. Chawanonphithak, K., C. Phongcharoenpanich, S. Kosulvit, and M. Krairiksh, "Characteristics of an elliptical ring antenna excited by a linear electric probe," *International Journal of Electronics*, Vol. 94, No. 10, 973–984, 2007.
11. Risser, J. R., *Microwave Antenna Theory and Design*, McGraw Hill, 1949.
12. Yaghjian, A., "Approximate formulas for the far field and gain of open-ended rectangular waveguide," *IEEE Transactions on Antennas and Propagations*, Vol. 32, No. 4, 378–384, 1984.
13. Jia, H., K. Yoshitomi, and K. Yasumoto, "Rigorous analysis of

rectangular waveguide junctions by fourier transform technique," *Progress In Electromagnetics Research*, PIER 20, 263–282, 1998.

14. El Sabbagh, M. and K. Zaki, "Modeling of rectangular waveguide junctions containing cylindrical posts," *Progress In Electromagnetics Research*, PIER 33, 299–331, 2001.
15. Booty, M. R. and G. A. Kriegsmann, "Reflection and transmission from a thin inhomogeneous cylinder in a rectangular TE_{10} waveguide," *Progress In Electromagnetics Research*, PIER 47, 263–296, 2004.
16. Liang, J.-F., H.-C. Chang, and K. A. Zaki, "Coaxial probe modeling in waveguides and cavities," *IEEE Transactions on Microwave Theory and Techniques*, Vol. 40, No. 12, 2172–2180, 1992.
17. Yao, H.-W. and K. A. Zaki, "Modeling of generalized coaxial probes in rectangular waveguides," *IEEE Transactions on Microwave Theory and Techniques*, Vol. 43, No. 12, 2805–2811, 1995.
18. Tai, C. T., *Dyadic Green Functions in Electromagnetic Theory*, 2nd Edition, IEEE Press, 1994.
19. Tai, C. T., "On the eigenfunction expansion of dyadic Green's function," *The Proceedings of IEEE*, Vol. 61, 480–481, 1973.
20. Moroney, D. T. and P. J. Cullen, "The Green's function perturbation method for solution of electromagnetic scattering problems," *Progress In Electromagnetics Research*, PIER 15, 221–252, 1997.
21. Liu, S., L. W. Li, M. S. Leong, and T. S. Yeo, "Rectangular conducting waveguide filled with uniaxial anisotropic media: A modal analysis and dyadic Green's function," *Progress In Electromagnetics Research*, PIER 25, 111–129, 2000.
22. Rao, S. M., D. R. Wilton, and A. W. Glisson, "Electromagnetic scattering by surfaces of arbitrary shape," *IEEE Transactions on Antennas and Propagation*, Vol. 30, 409–418, 1982.
23. Volakis, J. L. and D. B. Davidson, "Moment antenna simulation with matlab: RWG basis functions," *IEEE Antennas and Propagation Magazine*, Vol. 43, No. 5, 100–107, 2001.
24. Makarov, S. N., *Antenna and EM Modeling with MATLAB*, John Wiley & Sons, 2002.
25. Hanninen, I., M. Taskinen, and J. Sarvas, "Singularity subtraction integral formulae for surface integral equations with RWG, rooftop and hybrid basis functions," *Progress In Electromagnetics Research*, PIER 63, 243–278, 2006.